Semiconductor Optoelectronics
ISSN: 1001-5868

STRUCTURE, MAGNETIC AND DIELECTRIC PROPERTIES OF MG-CO-CU NANO FERRITE POWDER SYNTHESIZED BY SOL-GEL AUTO COMBUSTION METHOD.

M.Manikandan[1], N. Sundaramurthy[1,2], S. Rajalakshmi[3]
[1]Department of Physics, Annamalai University, Annamalai Nagar, Tamilnadu, India.
[2]Thiru Kolanjiappar Government Arts College, Virddhachalam.
[3]University College of Engineering panruti, Panruti.

Abstract:

The sol-gel auto-combustion process was utilized to create Mg-Co-Cu ferrite nanoparticles with the chemical formula $Mg_{0.5}Co_{0.25}Cu_{0.25}Fe_2O_4$. The XRD patterns of the prepared sample confirm the composition of the spinel phase cubic spinel structured nanoparticles. By using Fourier transform infrared (FTIR) measurements, the creation of the spinel structure was also verified. Images obtained using field emission scanning electron microscopy show that spherically cubic-shaped particles exist. Mg, Co, Cu, Fe, and O were the primary constituents of $Mg_{0.5}Co_{0.25}Cu_{0.25}Fe_2O_4$, which energy dispersive X-ray (EDX) analysis revealed to have a pure phase and structure. UV-diffuse reflectance studies were used to describe the optical properties of this ferrite nanoparticle (UV-DRS). The optical band gap was determined from UV-DRS to be in the range of 1.76eV. Cation distribution of spinel ferrite nanoparticles confirmed by X-ray photoelectron spectroscopy (XPS). Using a vibrating sample magnetometer, the magnetic characteristics were employed and measured (VSM). By observing the sample's hysteresis loop, their ferromagnetic property was established. The frequency was shown to be inversely correlated with the dielectric parameters, including the dielectric constant (ε′), and dielectric loss (ε′′). In addition, it was discovered that the frequency increased the A.C conductivity of Mg-Co-Cu nano ferrites.

Keywords: Sol-gel auto combustion, XPS, VSM, FESEM, UV-DRS, Dielectric study

1. Introduction:

Iron oxide and metal oxide are magnetic ceramics known as ferrites, which will be used in future permanent magnets, memory storage units, microwave devices, and telecommunications equipment. Ferrites are particularly good at electrical and magnetic properties such as strong electrical resistivity, low dielectric loss, high saturation magnetization, high permeability, and moderate permittivity [1-3]. Ferrites in the nanocrystalline form are important in emerging sectors such as magnetically assisted medication delivery, magnetic resonance imaging, catalysis, magnetic fluids, and humidity and gas sensors. Three forms of ferrites are hexagonal ferrite, garnet ferrite, and spinel ferrite which can be distinguished depending on the crystal structure. Spinel ferrite is a regular combination of oxygen with the usual chemical formula AB_2O_4. The unit cell of spinel ferrites has 32 oxygen atoms dispersed in tetrahedral (A) and octahedral (B) sites in a cubic closed pack [4-6]. Spinel nanocrystalline ferrites' chemical and

structural characteristics are very dependent on their composition and the synthesis techniques used, and the cation substitutions that make up those attributes affect the related electric and magnetic properties. Because of its great magneto-crystalline anisotropy and high saturation magnetization, the inverse type of spinel ferrites is the most intriguing.

According to the literature, there are a large number of both traditional and unconventional ways to spread an idea, including the solid-state approach (7), the sol-gel self-igniting route (8), a hydrothermal technique (9), the microemulsion route (10), and the co-precipitation methodology (11). which have been effectively employed to regulate the characteristics of spinel ferrites. The primary shortcomings of conventional techniques. Are issues with limited reproducibility, using high temperatures, and contamination. Therefore, fresh preparation methods have emerged recently to satisfy the demands of the time. Numerous investigations have been done on the effects of Co [12], Cu [13], Co-Mg [14], Mg-Zn-Co [15], Co-Mg [16], Co-Cu [17], and Cu-Mg [18]. These dopant ions affect ferrites' structural, optical, electrical, and magnetic properties. Few publications on Mg-Co-Cu nano ferrite powder have been published, at least according to the best of our search. In Co-Ferrites ($CoFe_2O_4$), UV-Vis spectroscopy revealed two optical band gaps at 4.1 eV and 4.9 eV. Furthermore, it was found that as the temperature rose, the resistance decreased. $CuFe_2O_4$ was made by Raja et al. using the sol-gel and microwave methods. Comparative investigations found that the size of the particles affected the magnetic characteristics. The saturation magnetization of Cu_2^+ ferrite produced through the sol-gel method was 42.23 emu/g. Using the self-igniting method, polycrystalline Cu1-xCoxFe$_2$O$_4$ nanoparticles were created, and it was discovered that the lattice constant increased when Co_2^+ cations were included. According to the VSM analysis, the magnetic properties grew as the Co_2^+ cation concentration did. Co-Cu ferrite reaches its greatest saturation magnetization (66.1 emu/g) and coercivity (960 Oe) when x = 0.9.

The sol-gel auto combustion approach was used in this study to create nano-sized $Mg_{0.5}Co_{0.25}Cu_{0.25}Fe_2O_4$ferrite powder while optimizing its structural, optical, electrical dielectric, ferroelectric, and magnetic properties. Several characterization techniques were used to investigate the characteristics of the generated samples Mg-Co-Cu nano ferrites powder, such as XRD, FESEM, UV-DRS, VSM, and dielectric studies.

2. Experimental method.

2.1 Materials used and synthesis method

As initial components, highly pure analytical reagent (AR) grade compounds, such as Magnesium (II) [Mg $(No_3)_{2.6}H_2O$] nitrate hexahydrate (), Cobalt (II) [Co $(No_3)_{2.6}H_2O$] nitrate hexahydrate (98.0%), Copper (II) [Cu $(No_3)_{2.3}H_2O$] nitrate trihydrate (99.99%), Iron (III) [Fe $(No_3)_{3.9}H_2O$] nitrate nonahydrate (99.95%). Citric ($C_6H_8O_7$) acid was chosen as the fuel agent to synthesize the Mg-Co-Cu ferrite powder. The stoichiometric calculations maintained the metal nitrates to citric acid mole ratio at 1:3. A magnetic stirrer operating at a constant 50 rev/min speed was used to mix the solution. As the stirring process continued, ammonia (NH3) solution was added to achieve a pH of 7 while keeping the temperature at 353 k. The mixture was first turned into a gel, which was then burned in an auto-combustion process to create a fluffy loose powder. The produced powder was calcined at 873K for 2 hours, sintered at 1273K for 2 hours, and then milled to obtain a fine powder. The procedure is depicted graphically in Fig. 1.

2.2 characterization techniques.

The structural as-prepared Mg-Co-Cu ferrite powder was characterized via XRD (X' pert pro -Panalytic, Cu-Kα radiation, and λ = 1.54060 Å) to obtain Bragg angle (2θ) range 20˚-80˚. CARL ZEISS –SIGMA 300 is used to study surface morphology and investigate size and shape. UV – Diffuse Reflectance Spectrometer (UV-DRS) model SHIMADZU/ UV 2600, was taken to measure the as-prepared samples. Fourier transform spectroscopy (FTIR) identified the surface properties of the sample. VSM (Lakeshore cryotronics, Inc., US) was employed to reckon the magnetic performance parameters of the samples at room temperature. Model K-alpha-KAN9954133 XPS was applied to investigate the surface composition of the sample. The frequency dependence of dielectric permittivity and dielectric losses were studied using NOVOCONTROL Technologies GmbH & Co. Germany Model: Concept 80.

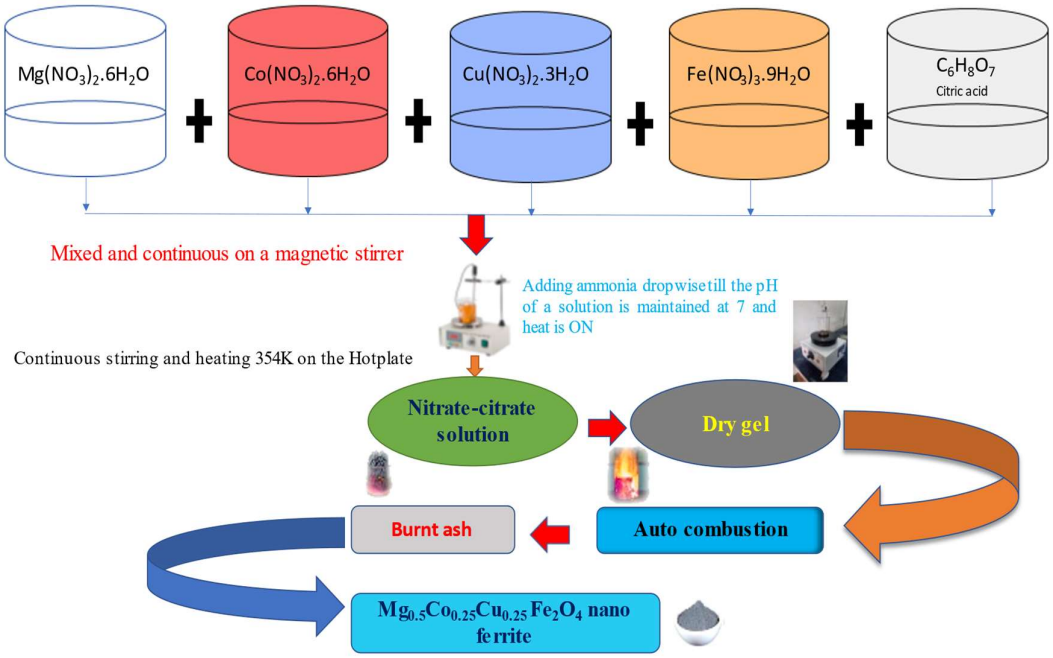

Fig. 1. Schematic diagram of the synthesis of Mg-Co-Cu nano ferrite powder.

3. Result and Discussion

The characterization method was used to prepare $Mg_{0.5}Co_{0.25}Cu_{0.25}$ Fe_2O_4 nano ferrite powder. The next subsections explain the results of the characterization procedures in detail.

3.1 X-ray diffraction (XRD)

The typical X-ray diffraction pattern of the Mg0.5Co0.25Cu0.25Fe2O4spinel ferrite nanoparticles is shown in fig.2. The XRD pattern shows the reflections belonging to the cubic structure, and matches with (JCPDS card 73-2410) no extra peaks have been observed in the XRD patterns. The single-phase formations of compounds under investigation were confirmed from the analysis of the XRD pattern. The intensity of the (311) plane is more as compared to other planes like (220), (400), (422), (511), and (440) and is chosen for the determination of crystallite size. Table 1 gives the planes (h k l), corresponding to Bragg's angles along with their interplanar spacing (d) values, intensity, and intensity ratio of the $Mg_{0.5}Co_{0.25}Cu_{0.25}Fe_2O_4$ferrite system.

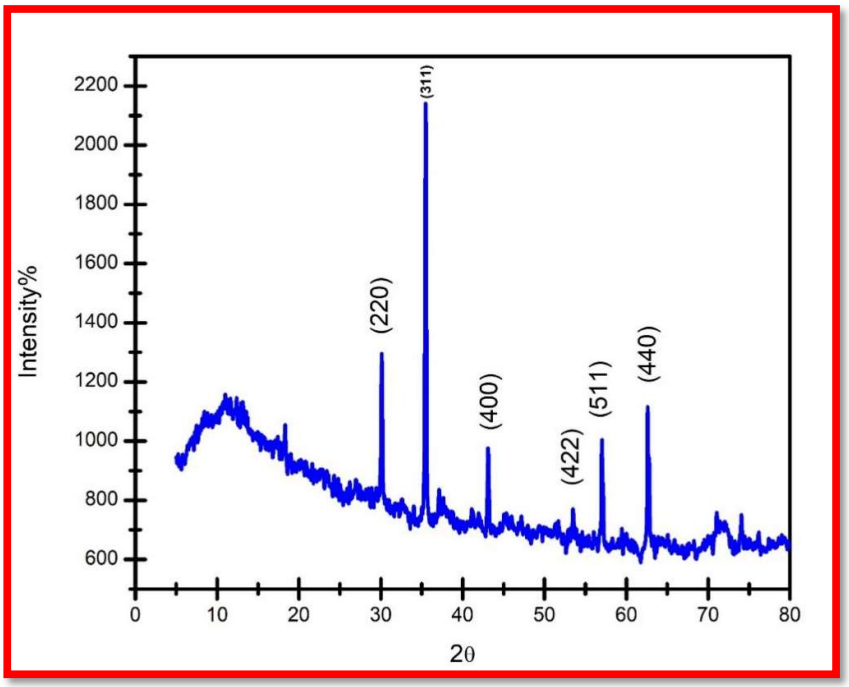

Fig. 2. XRD spectra of $Mg_{0.5}Co_{0.25}Cu_{0.25}Fe_2O_4$ ferrites powder

Using the interplanar spacing (d) and the corresponding Miller indices, the lattices constant (a) of all the samples were calculated using standard relation,

$$a = d\sqrt{(h^2+k^2+l^2)} \qquad (1)$$

where d is interplanar spacing and (h k l) are miller Indices. The obtained values of the lattice constant 'a' are given in table 1. The unit cell Volume (v) for both the samples was calculated by using the following equation and is represented in table 1.

$$V = a^3 \qquad (2)$$

The values of lattices constant and molecular weight (table.1) were used to determine the X-ray density for all the samples. The X-ray density was calculated using the following relation [19].

$$dx = \frac{Z\times M}{V\times Na}\text{gm/cm}^3 \qquad (3)$$

where d is X-ray density, Z is the number of molecules per unit, M is the molecular mass of the sample, V is the unit cell volume, and Na is Avogadro's number. The crystallite size of the samples was calculated using Debye-Scherer's formula as given below [20]. The plane (311) with maximum intensity was considered for fullwidth at half maxima (FWHM), the obtained values of crystallite size given in table 1 suggest that the prepared samples have nanocrystalline nature.

$$D = 0.9\lambda/\beta \cos\theta \qquad (4)$$

where λ is the wavelength of the Cu-Kα radiation, β is the full width of the half maximum and θ is Bragg's angle. The average particle size is shown in Table 1

$$\delta = 1/D^2 \qquad (6)$$

The hopping lengths L_A and L_B, respectively, provide information about the separation among oxygen ions and tetrahedral (A-) and octahedral (B-) cations. Moving charge transmits from one lattice site to an additional one requires a greater potential when the hopping length is big, but moving charge carriers into the sublattices requires a lower potential when the hopping length is small [21]. To define the hopping lengths of L_A and L_B, relationships (6) then (7) were used. [21];

$$L_A = \frac{a\sqrt{3}}{4} \qquad (7)$$

$$L_B = \frac{a\sqrt{2}}{4} \qquad (8)$$

In Table 1, the "L_A" and "L_B" values for the prepared samples are given. Many researchers employed a variety of techniques to learn how cations were distributed [22-24]. Table 2 provides the cation distribution. The following hypotheses determine these cation arrangements: a) The total number of cationic setups is one at the A-site and two at the B-site. b) The spinel matrix has zero overall charges. Therefore, the positive and negative charges in the combination must be equivalent to building an electrically neutral structure. The crystal structure of magnesium ferrite is partially inverse spinel [25]. Partially inverse spinel exists in cobalt and copper ferrites [26] and Mg^{2+}, Co^{2+}, Cu^{2+}, and Fe^{3+} cations occupy mutually the A- and B- sites [27]. The ionic radii "r_A" and "r_B" at the A- and B-sites were calculated for all of the synthesized ferrites using the cationic distribution (Table 2) equations (8) and (9).

$$r_A = (C_{Mg^{2+}})\,(r_{Mg^{2+}}) + (C_{Co^{2+}})\,(r_{Co^{2+}}) + (C_{Cu^{2+}})\,(r_{Cu^{2+}}) + (C_{Fe^{3+}})\,(r_{Fe^{3+}}) \qquad (9)$$

$$r_B = \tfrac{1}{2}\,[\,(C_{Mg^{2+}})\,(r_{Mg^{2+}}) + (C_{Co^{2+}})\,(r_{Co^{2+}}) + (C_{Cu^{2+}})\,(r_{Cu^{2+}}) + (C_{Fe^{3+}})\,(r_{Fe^{3+}})] \qquad (10)$$

where $(C_{Mg^{2+}})$, $(C_{Co^{2+}})$, $(C_{Cu^{2+}})$, and $(C_{Fe^{3+}})$ represent the concentration of Mg^{2+}, Co^{2+}, Cu^{2+}, and Fe^{3+} taken at the A-site and B-site according to cation distribution while rMg^{2+} = tet.:0.57Å and oct.:0.72Å [28] rCo^{2+} = tet.:0.58Å and oct.:0.745Å, and rFe^{3+}= tet.: 0.49 Å and oct.: 0.645 Å [29], rCu^{2+} tet.:0.57Å and oct.:0.73Å [30], are the cationic radii of Mg^{2+}, Co^{2+}, Cu^{2+}, and Fe^{3+} cations, respectively. The evaluated ionic radii values for octahedral (r_B) and tetrahedral (r_A) sites are listed in Table 2. The theoretical lattice constant (*ath*) was defined *via the* following equation [31];

$$ath = \frac{8}{\sqrt[3]{3}}\,[\,(r_A + R_0) + 1.73\,(r_B + R_0)] \qquad (11)$$

where R_0 = 1.32 Å is the ionic radii of oxygen. Table 2 contains the values of "ath." Utilizing the relation, the oxygen positional parameter (u) was calculated. (12) [32];

$$u = (r_A - R_0)\,\frac{1}{\sqrt{3}a} + 1/4 \qquad (12)$$

Table 3 showed that the synthesis and sintering procedures lead to a modest change of "u" from

its ideal value of 0.375 Å, which is indicated by the alternation in anion dislocation from the perfect structure. The bond lengths between the A-site (R_A) and B-site (R_B) were calculated using [32];

$$R_A = (u - 0.25)\,(a\sqrt{3}) \quad (13)$$

$$R_B = a\sqrt{(3u^2 - \frac{11}{4}u + \frac{43}{64})} \quad (14)$$

$$d_{BL} = \sqrt{2}\,(2u - \frac{1}{2})\,a \quad (15)$$

$$d_{BLU} = (\sqrt{4u^2 - 3u + \frac{11}{16}})\,a \quad (16)$$

$$d_{AL} = \sqrt{2}\,(2u - \frac{1}{2})\,a \quad (17)$$

In Table 3, there is a list of the values for "R_A" and "R_B." Tetrahedral edge lengths (d_{AL}), unshared octahedral edge lengths (d_{BLU}), and shared octahedral edge lengths (d_{BL}) were all calculated using relationships; bond edge length values are shown in Table 3.

Table 1. Calculated parameters from XRD analysis of $Mg_{0.5}Co_{0.25}Cu_{0.25}Fe_2O_4$ nano ferrite.

Sample	Lattice parameters a (Å)	Average crystallite size (nm)	X-ray density (d_x) gm/cm^3	Cell volume (Å^3)	d (Å)	δ (line/m^2)	L_A (Å)	L_B (Å)
$Mg_{0.5}Co_{0.25}Cu_{0.25}Fe_2O_4$	8.3865	81	4.495	589.85	2.5300	1.52	3.6313	2.9646

Table 2. cationic scattering at sub-lattice A and B sites, tetrahedral and octahedral ionic radii (r_A and rB), the theoretical lattice constant (*ath*)

Samples	r_A (Å)	r_B (Å)	ath (Å)
$Mg_{0.5}Co_{0.25}Cu_{0.25}Fe_2O_4$	0.7762	0.6726	8.5407

Table 3. Oxygen parameters (u), bond length (RA, RB), and Bond edge lengths (d_{AL}, d_{BL}, d_{BLU}) for the prepared ferrites.

Samples	Oxygen position parameter	Bond lengths (Å)		Bond edge lengths (Å)		
		R_A	R_B	d_{AL}	d_{BL}	d_{BLU}
$Mg_{0.5}Co_{0.25}Cu_{0.25}Fe_2O_4$	0.3917	2.0961	2.0011	2.6161	3.4229	3.0328

3.2 Morphological properties.

The field emission scanning electron microscope (FESEM) images of the $Mg_{0.5}Co_{0.25}Cu_{0.25}Fe_2O_4$ferrite sample at an enhancement of 200nm are depicted in fig. 3 from the figure shows the presence of particles that are agglomerated together. A close observation would reveal the presence of particles showing cubic faces. The distribution of particles is uniform and it can be seen that the particle is well below the size of 100nm. This supports our prediction of grain size determined using Scherrer's formula.

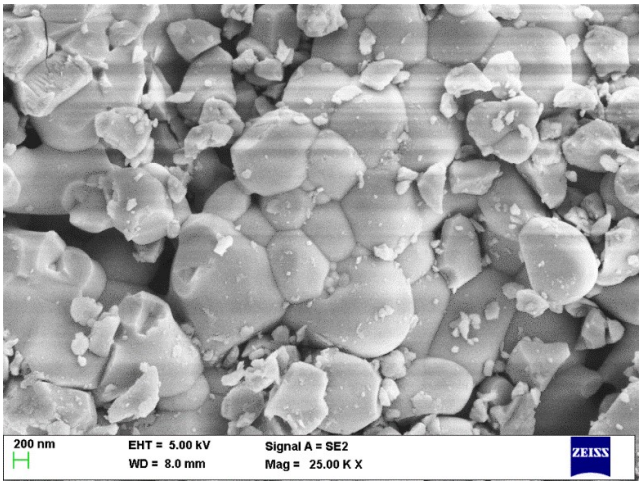

Fig. 3. FESEM image of $Mg_{0.5}Co_{0.25}Cu_{0.25}Fe_2O_4$ ferrites powder

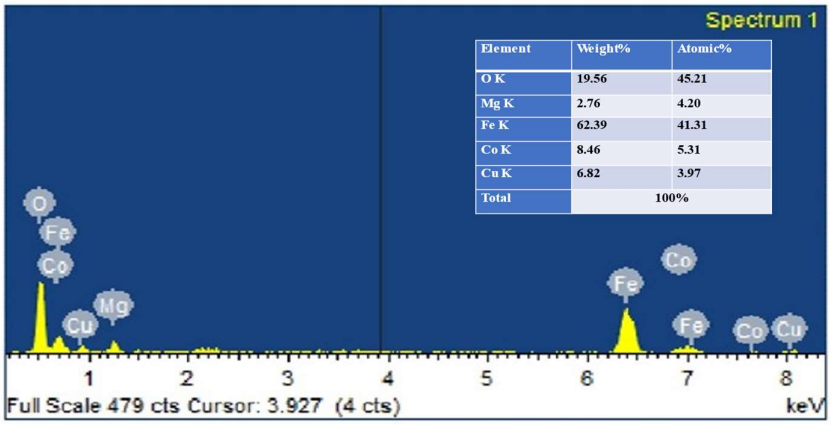

Fig. 3a. EDX pattern of $Mg_{0.5}Co_{0.25}Cu_{0.25}Fe_2O_4$ ferrites powder

The ingredient of the constituent elements of the synthesized nanoparticles was studied and analyzed by using energy dispersive X-ray (EDX). EDX spectra of pure Mg-Co-Cu ferrite sample of $Mg_{0.5}Co_{0.25}Cu_{0.25}Fe_2O_4$are shown in fig 4. the four components of Mg, Co, Cu, Fe, and O were measured in a pure Mg-Co-Cu-ferrite sample have a pure phase and structure.

3.3 FT-IR measurement

The FT-IR spectrum of a spinel structure recorded in the wave number range of 4000 cm^{-1} to 400 cm^{-1} is anticipated to contain two main broad metal-oxygen bands, one (ν_1) in the range of 600 cm^{-1} to 550 cm^{-1} due to the stretching vibrations of the tetrahedral metal-oxygen bond and the other (ν_2) in the range of 450 cm^{-1} to 385 cm^{-1} due to the octahedral metal-oxygen

bond [21]. Figure 4 is the FTIR spectrum of $Mg_{0.5}Co_{0.25}Cu_{0.25}Fe_2O_4$, which confirms the spinel structure of the synthesized Mg-Co-Cu ferrite by showing the existence of ν_1 vibration [Fe-O] at 584cm^{-1} and ν_2 vibration [Mg-O] at 430 cm^{-1}. The O-H stretching vibration interacting via H bonds is what causes the powerful wide band at spectra 3450 cm^{-1} and the less intense band around spectra 1620 cm^{-1} in the spectra is caused by O-H stretching vibration interacting with H bonds. The force constant (K) was defined by the following relation [33].

$$K = 4\pi^2 \nu^2 c^2 m \qquad (18)$$

Where m, c, and ν represent the reduced mass, speed of light, and wavenumber, respectively. Table 4 provides the divalent cation's force constants at the octahedral (K_0) and tetrahedral (K_T) sites.

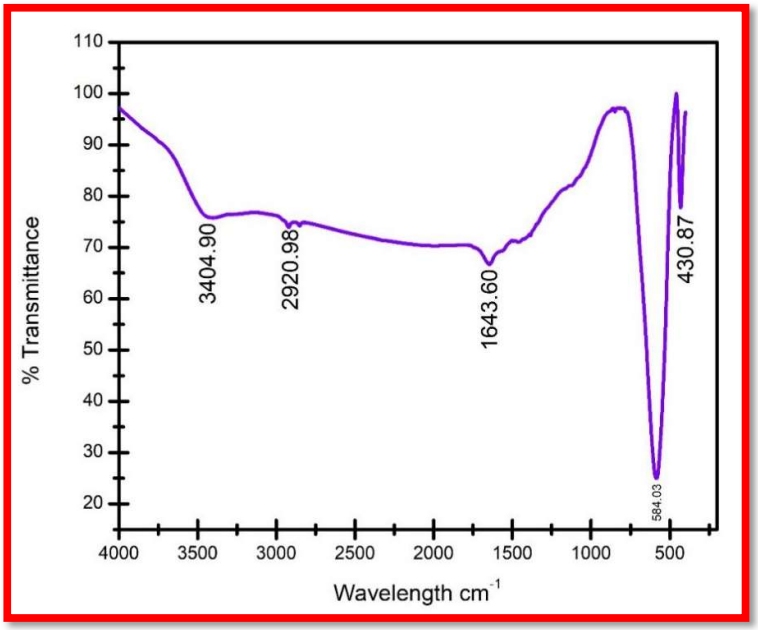

Fig. 4. FT-IR spectrum of $Mg_{0.5}Co_{0.25}Cu_{0.25}Fe_2O_4$ ferrite powder.

Table 4. FTIR parameters of the as-synthesized samples.

Samples	ν_T cm^{-1}	ν_O cm^{-1}	K_T × 10^5 (dyne/cm^{-1})	K_O × 10^5 (dyne/cm^{-1})
Mg0.5Co0.25Cu0.25Fe2O4	584.03	430.8	2.496704	1.054248

3.4 UV-Drs analysis

The pure Mg-Co-Cu ferrite NPs are investigated by UV-DRS spectroscopy fig. (6) shows the reflectance spectra of pure Mg-Co-Cu nano ferrite. The band gap energy of the synthesized sample is derived from the optical reflectance data using the Kubelka-Munk function [22,23]

$$F(R) = (1-R)^2/2R \qquad (5)$$

Where R is the diffuse reflectance. The direct band gap value of the prepared sample is estimated by the graph plotted between $[F(R)\ h\nu]^2$ and hν and the intercept obtained is the band

gap energy fig.5. The $Mg_{0.5}Co_{0.25}Cu_{0.25}Fe_2O_4$for the pure band gap is 1.76 eV. The band gap energy with increasing calcination temperature probably attributes to the crystallite growth of synthesized yield.

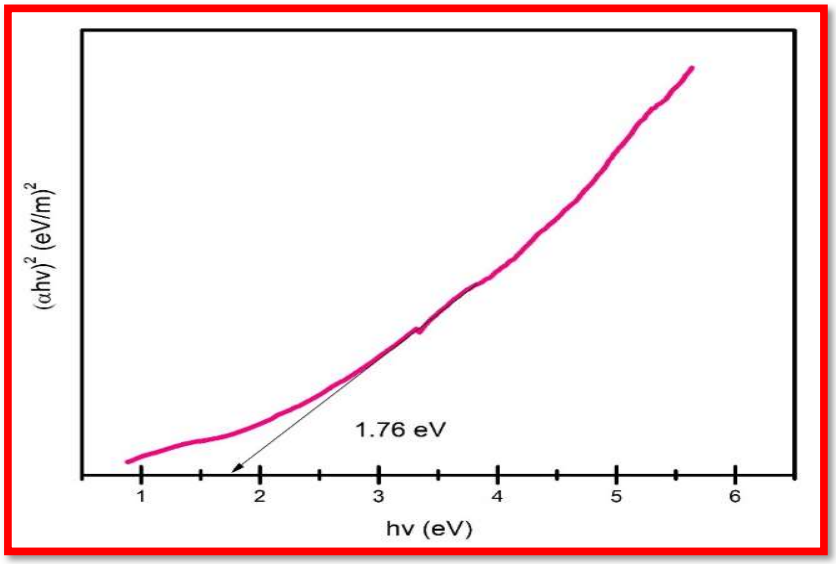

Fig. 5. UV-Visible diffuse reflectance spectra of $Mg_{0.5}Co_{0.25}Cu_{0.25}Fe_2O_4$

3.5 X-ray photoelectron spectroscopy (XPS)

In a synthesized sample of Mg-Co-Cu ferrite, the oxidized states of Mg, Co, Cu, and Fe can be identified by X-ray photoelectron spectroscopy (XPS). The X-ray photoelectron spectroscopy (XPS) of $Mg_{0.5}Co_{0.25}Cu_{0.25}Fe_2O_4$ nano ferrite particle composed of citric acid was shown in fig 6(a). The binding energy of Mg1s, Co2p, Cu2p, and Fe 2p established the existence of magnesium, cobalt, copper, and irons ions in the synthesized ferrite nanoparticles. From Fig 6 (b), the peaks of 1303eV can be allocated to Mg1s, while the same peaks in MgFe2O4 occur at eV [24]. Fig 6 (c) shows that the binding energy 933.4 and 953,2eV correspond to $Cu2p_{3/2}$ and $Cu2p_{1/2}$, and the satellite peak Cu_2^+ is 941.6eV [25,26]. In the XPS spectrum of Co2p, the peaks for $Co2p_{3/2}$ and $Co2p_{1/2}$ are in the binding energy of 779.8 and 795.2 eV respectively these are standard Binding energy signals for the Co_2^+ state [27]. Fe2p, the distinct peaks of Fe2p3/2 and Fe2p1/2 are approached at 710.0 and 724.1 eV respectively [28]. The XPS spectrum of O1s shows signals closed in 529.2 eV ascribed to the lattice oxygen and the binding energy signal at 530.8 eV is due to the existence of oxygen defects [29].

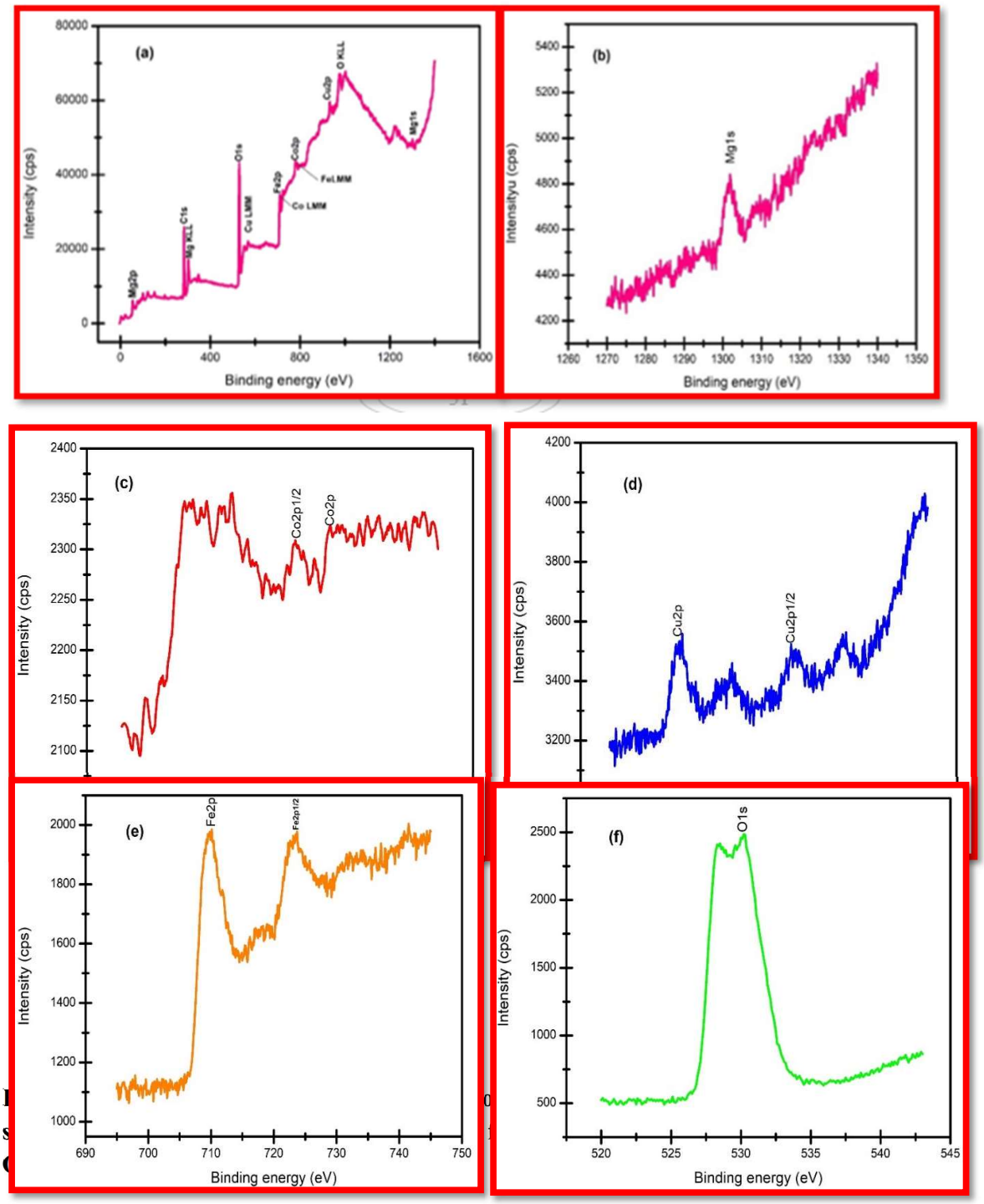

3.4. VSM ANALYSIS

It is analyzed using a vibrating sample magnetometer (VSM) to interpret the magnetic properties of nano ferrite. The hysteresis loop detected at room temperature for $Mg_{0.5}Co_{0.25}Cu_{0.25}Fe_2O_4$is shown in fig.7. The values of the saturation magnetization (Ms), coercivity (Hc), and retentivity (Mr) are attained. The magnetic parameters were calculated in concurrence with the data given in table.5 and the following formula is given as follows. The

investigational values of the magnetic moment (μ_B) per formula per unit in Bohr magneton are calculated using the following relationships [30]

$$\mu_{B(exp)} = \frac{Mw \times Ms}{5585} \qquad (6)$$

where M_w is the molecular weight of the $Mg_{0.5}Co_{0.25}Cu_{0.25}Fe_2O_4$and Ms is the saturation magnetization of the sample.

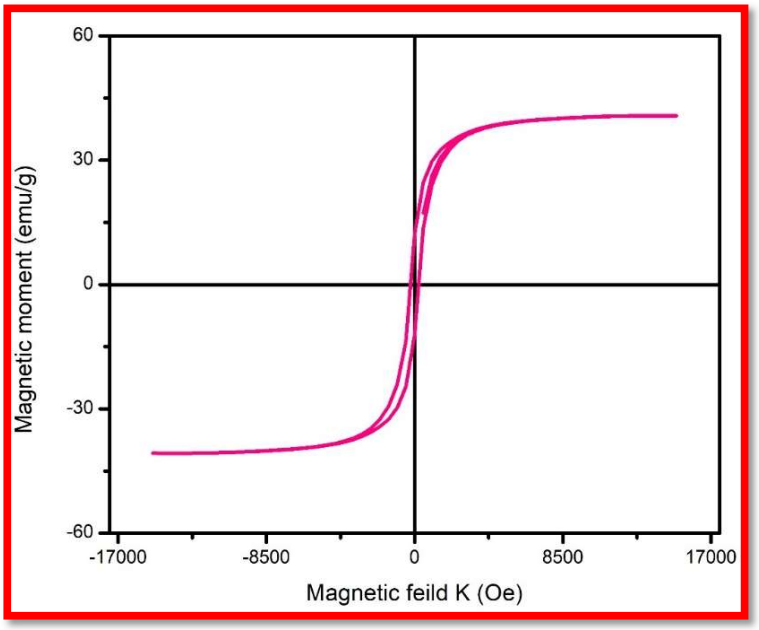

Fig. 7. Hysteresis loop for $Mg_{0.5}Co_{0.25}Cu_{0.25}Fe_2O_4$.

The values of Magnetic variables such as Ms, Hc, and Mr of nanoparticles of Mg-Co-Cu-Fe_2O_4 obtained from the VSM data are 40.68 emu/g, 234.91G, and 12.06 emu/g, respectively. Huang et al. [31] have reported a coercivity value of 165 G for 10nm particles. [32] have reported a Hc value of 576Oe for a particle size of 80nm. A correlation of these data resolves a directly proportional relationship between coercivity and particle size, which is an impact of the nano regime.

it is an accepted principle [33] for bulk particles that grain size and coercivity have reciprocal relations. It is explained that nano ferrite particles having tens of nanometre dimensions are considered to have single domains. although a smaller coercive field is normally assumed to be caused by multidomain for bulk particles, i.e., in the nano regime there is a changeover from multidomain nature to single-domain nature. The maximum value of coercivity of nanoparticles is ascribed to the demagnetization caused by domain rotation (single-domain), which needs greater energy rather than the movement of the walls (multidomain).

Table. 5. magnetic parameters of the prepared ferrite sample.

Sample	Remanent Magnetization, M_r (emu/g)	Saturation magnetization, M_s (emu/g)	Coercivity, H_c (O_e)	Squareness, S (M_r/M_s)	Magnetic moment (μ_B)
Mg-Co-	17.368	40.685	234.01	0.4268	1.456

Cu-Fe_2O_4					

3.5 Dielectric and a.c conductivity studies.

The impact of frequency f on the dielectric parameters such as dielectric loss (tan δ), and dielectric constant (ε′) are studied in the frequency range at room temperature. The dielectric parameters (tan δ, ε′) are observed to decrease with the increase in the frequency. This is the normal dielectric functioning of ferrites, which was mentioned before for other nano ferrites at room temperature [34,35].

Fig. 8b. shows the variation of dielectric loss tangent (tan δ) with log frequency for the Mg-Co-$CuFe_2O_4$ sample. The dielectric loss tangent is observed to decrease with the increase in frequency. The drop in the tan δ is rapid at low frequencies and becomes slow at higher frequencies. As Iwauchi [36] mentioned, there is a strong connection between the conduction mechanism and the dielectric efforts of ferrites. The decrease in the dielectric tangent is vary in frequency in the present studies following the Koops phenomenological model [37].

The form of dielectric constant (ε′) with frequency at room temperature is shown in fig.8. From the plot it can be seen that the dielectric constant initially decreases rapidly with an increase in frequency but beyond 100KHz remains fairly constant in fig.8a. The variation found in the dielectric constant with the frequency is assigned to the fact that the electron exchange between Fe_2^+ and Fe_3^+ ions cannot follow the change of the externally applied field apart from a certain frequency. The discover dielectric loss pattern is seen to be the most important part of the total core loss in ferrite [38,39]. The state dielectric loss pattern is seen to be similar to that of the dielectric constant and dielectric loss tangent. Thus, the dielectric constant and dielectric loss acquired for the present nano ferrites synthesized by the combustion method possesses a lower value than that of the ferrite prepared by the conventional ceramic method for the same composition. The low dielectric values make these ferrites to be used in higher frequency applications.

The a.c conductivity analyses were taken on over a wide range of frequencies [40] for Mg-Co-Cu nano ferrite. The difference of a.c conductivity (σ) with the frequency is shown in fig. 8.c. As the applied frequency is high the a.c conductivity of the Mg-Co-Cu nano ferrite is observed to increase exponentially. The electrical conduction mechanism in the Mg-Co-Cu nano ferrite is in line with the electron hopping model.

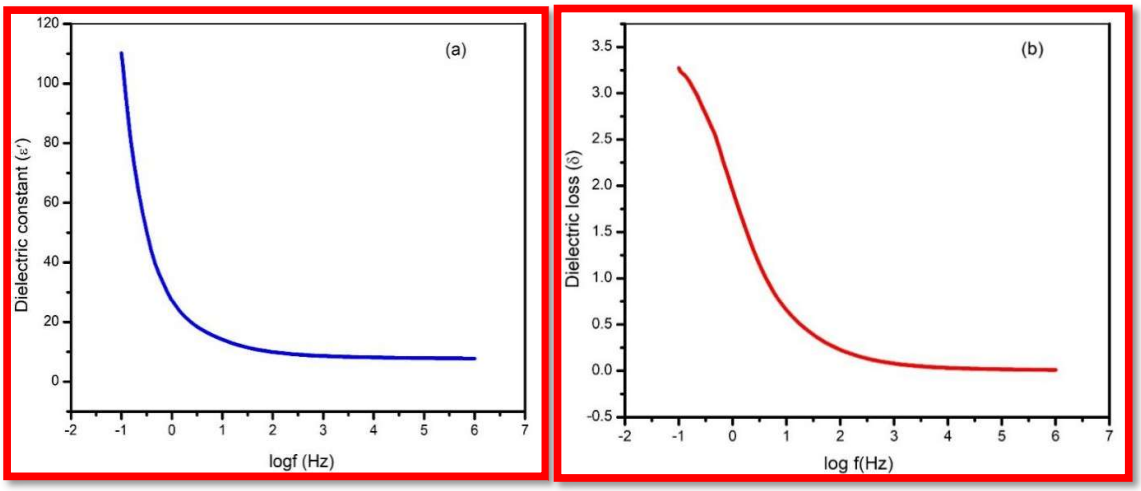

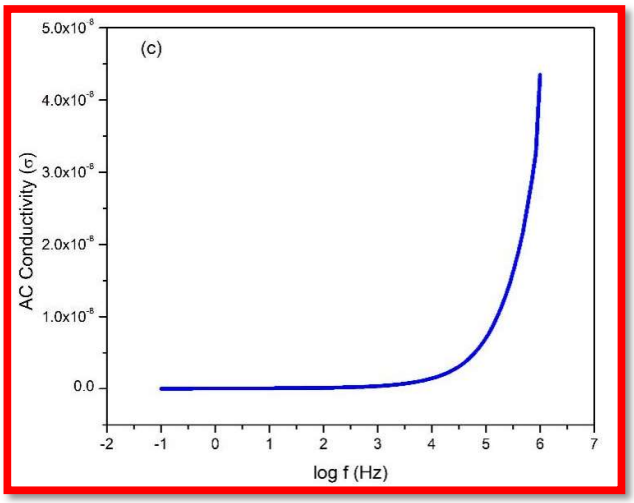

Fig. 8. a) variation of dielectric constant (ε′) with frequency. (b) Variation of dielectric loss factor (ε′′) with frequency. (c) variation a. c. conductivity (σ) with the frequency

4. Conclusion.

This investigation of prepared Mg-Co-Cu nano ferrite powder via a sol-gel auto combustion route. The nitrate-citrate gels reveal a self-propagation nature after reacting with air. The crystalline quality of the produced sample was confirmed by X-ray diffraction patterns and the phase of the sample shows the cubic spinel structure of the material. The FESSEM micrographs show the cubic shape and EDAX spectra show the presence of Mg, Co, Cu, Fe, and O in Mg0.5Co0.25Cu0.25Fe2O4 nanoparticles. In FTIR spectrum shows main incorporate bands around 584 cm^{-1} and 430 cm^{-1}. UV-DRS study of Mg-Co-Cu nano ferrite reveals an optical band gap of 1.78eV. The XPS study established the presence of elements in the expected oxidation state. The magnetic variable like coercivity, retentivity, and the magnetic moment was measured using VSM. The AC conductivity increases with increase in frequnecy which was suitable in microwave device applications.

Reference

1. H.E. Zhang, B.F. Zhang, G.F. Wang, X.H. Dong, Y. Gao, The structure and magnetic properties of $Zn_{1-x}Ni_xFe_2O_4$ ferrite nanoparticles prepared by sol-gel auto-combustion, J. Magn. Magn Mater. 2007; 312: 126–130. https://doi.org/10.1016/j.jmmm.2006.09.016

2. Adrian I. Borhan, Vasile Hulea, Alexandra R. Iordan, Mircea N. Palamaru, Cr^{3+} andAl^{3+} co-substituted zinc ferrite: structural analysis, magnetic and electrical properties, Polyhedron 70 2014; 110–118. https://doi.org/10.1016/j.poly.2013.12.022

3. Sonal Singhal, Kailash Chandra, Cation distribution and magnetic properties in chromium-substituted nickel ferrites prepared using aerosol route, J. Solid StateChem. 2007; 180: 296–300. https://doi.org/10.1016/j.jssc.2006.10.010

4. K. Vijaya Babua, G.V. Santosh Kumara, K. Jalaiahb, Paulos Teddesse Shibeshic Effects of copper substitution on the microstructural, electrical, and magnetic properties of $Ni_{0.7}Co_{0.3-}$

$_xCu_xFe_2O_4$ ferrites Journal of Physics and Chemistry of Solids 2018; 118: 172–18. https://doi.org/10.1016/j.jpcs.2018.02.051

5. Xiaohui Wang, Xucai Kan, Xiansong Liu, Shuangjiu Feng, Ganhong Zheng, Zhuhongbo Cheng, Wei Wang, Zuhua Chen, Chaocheng Liu Characterization of microstructure and magnetic properties for Co^{2+} ions doped $MgFe_2O_4$ spinel ferrites Materials Today Communications 2020; 25: 101-414 https://doi.org/10.1016/j.mtcomm.2020.101414

6. Ameer Azam, Microwave-assisted synthesis and characterization of Co-doped Cu ferrite nanoparticles Journal of Alloys and Compounds 2012; 540: 145–153. https://doi.org/10.1016/j.jallcom.2012.06.068

7. M. R. Barati, Characterization, and preparation of nanocrystalline Mg-Cu-Zn ferrite powders synthesized by sol-gel auto-combustion method J Sol-Gel Sci Technol 2009; 52: 171–178. https://doi.org/10.1007/s10971-009-2023-1

8. Lichao Yu and Aimin Sun, Influence of different complexing agents on structural, morphological, and magnetic properties of Mg–Co ferrites synthesized by sol-gel auto-combustion method J Mater Sci: Mater Electron 2021; 32: 10549–10563. https://doi.org/10.1007/s10854-021-05711-1

9. D.Mane, D.Birajdar, S.Patil, S.E.Shirsath, R.Kadam, Redistribution of cations and enhancement in magnetic properties of sol-gel synthesized $Cu_{0.7-x}Co_xZn_{0.3}Fe_2O_4$ ($0 \leq x \leq 0.5$), J. Sol. Gel Sci. Technol. 2011; 58: 70–79. https://doi.org/10.1007/s10971-010-2357-8

10. I.Ahmad, T.Abbas, M.Islam ,A. aqsood, Study of cation distribution for Cu–Co nano ferrites synthesized by the sol-gel method, Ceram.Int. 2013; 39: 6735–6741. https://doi.org/10.1016/j.ceramint.2013.02.001

11. G.Raja, S.Gopinath, R.A.Raj, A.K.Shukla, M.S.Alhoshan, K.Sivakumar, Comparative investigation of $CuFe_2O_4$ nano and microstructures for structural, morphological, optical and magnetic properties, Phys. ELow-dimens. Syst. Nanostruct. 2016; 83: 69–73. https://doi.org/10.1016/j.physe.2016.04.019

12. A.Singh, H.Gangwar, B.Dehiya, Synthesis and microstructural characterization of pure cobalt ferrite for DC electrical study, Journal of Material Science and Mechanical Engineering 2017; 4: 136–141.

13. C.Srinivas, E.R.Kumar, B.Tirupanyam, S.S.Meena, P.Bhatt, C.Prajapat, T.C.Rao, D.J.J.o.M.Sastry, M.Materials, Study of magnetic behavior in co-precipitated Ni–Zn ferrite

nanoparticles and their potential use for gas sensor applications, J.Magn. MagnMater. 2020; 502: 166534. https://doi.org/10.1016/j.jmmm.2020.166534

14. A.Scano, V.Cabras, M.Pilloni, G.Ennas, Microemulsions: the renaissance of ferrite-nanoparticle synthesis J.Nanosci.Nanotechnol. 2019; 19: 4824–4838. https://doi.org/10.1166/jnn.2019.16876

15. C.Aydin, H.Aydin, M.Taskin, F.Yakuphanoglu, A novel study: the effect of graphene oxide on the morphology, crystal structure, optical and electrical properties of lanthanum ferrite based nano electron ceramics synthesized by hydrothermal method, J.Nanosci. Nanotechnol. 2019; 19: 2547–2555. https://doi.org/10.1166/jnn.2019.15841

16. S.Prasad, M.Deepty, P.Ramesh, G.Prasad, K.Srinivasarao, C.Srinivas, K.V.Babu, E.R.Kumar, N.K.Mohan, D.J.C.I.Sastry, Synthesis of MFe2O4 (M=Mg^{2+}, Zn^{2+}, Mn^{2+}) spinel ferrites and their structural, elastic, and electron magnetic resonance properties, Ceram. Int. 2018; 44: 10517–10524. https://doi.org/10.1016/j.ceramint.2018.03.070

17. D.Mane, D.Birajdar, S.Patil, S.E.Shirsath, R.Kadam, Redistribution of cations and enhancement in magnetic properties of sol-gel synthesized $Cu_{0.7-x}Co_xZn_{0.3}Fe_2O_4$ ($0 \leq x \leq 0.5$), J.Sol. Gel Sci.Technol. 2011; 58: 70–79. https://doi.org/10.1007/s10971-010-2357-8

18. K.K.Bharathi, C.Ramana, Improved electrical and dielectric properties of La-doped ferrite, J.Mater. Res. 2011; 26: 584–591 https://doi.org/10.1557/jmr.2010.37

19. B.D. Cullity, S.R. Stock, Elements of X-ray diffraction. Pearson Education International, USA, 408 (2014)

20. Ali, M. B., Alsabah. Y. A., Siddig, M. A., Elbadawi, A. A., Ahmed, A. I. &Mirghni, A. A. Influenced of Cu^{2+}Doped on Structural, Morphological, and Optical Properties of Zn-Mg-Fe_2O_4 Ferrite Prepared by Sol-Gel Method. Advances in Nanoparticles, 2020; 9: 49-58 https://doi.org/10.4236/anp.2020.92004

21. Rita Sundari, Tang Ing Hua, ―The characterization study of ferrites (magnesium and manganese) using sol-gel method‖, The Malaysian Journal of Analytical Sciences, Vol. 18, Issue 3, 2014; pp. 485-490

22. A. Manikandan, J.J. Vijaya, L.J. Kennedy, M. Bououdina, Ceram. Int., 2013; **39:** 5909–5917 https://doi.org/10.1016/j.ceramint.2013.01.012

23. Kalai Selvan, R., Augustin, C.O., John Berchmans, L., Saraswathi, R.: Combustion synthesis of $CuFe_2O_4$. Mater. Res. Bull, 2003; 38: 41 https://doi.org/10.1016/S0025-5408(02)01004-8

24. J. Chastain, R.C. King Jr., Handbook of X-ray photoelectron spectroscopy, Perkin- Elmer Corporation 1992; 40: 221.

25. R.S. Yadav, I. Kuritka, J. Vilcakova, J. Havlica, J. Masilko, L. Kalina, et al., Structural, dielectric, electrical and magnetic properties of $CuFe_2O_4$nano-particles synthesized by honey mediated sol-gel combustion method and annealing effect, J. Mater. Sci. Mater. Electron. 2017; 28: 6245- 6261. https://doi.org/10.1007/s10854-016-6305-4

26. Y. Kang, L. Wang, Y. Wang, H. Zhang, Y. Wang, D. Hong, Y. Qv, S. Wang, Construction and enhanced gas sensing performances of CuO-modified-Fe_2O_3 hybrid hollow spheres, Sens. Actuators B. 2013; 177: 570-576. https://doi.org/10.1016/j.snb.2012.11.048

27. S.R. Naik, A.V. Salker, J. Mater. Chem. 22, 2740 (2012) https://doi.org/10.1039/C2JM15228B

28. Z. Gu, X. Xiang, G. Fan, F. Li, J. Phys. Chem. C 112, 18459 (2008) https://doi.org/10.1021/jp806682q

29. S.R. Naik, A.V. Salker, S.M. Yusuf, S.S. Meena, J. Alloys Compd., 2013; 54: 566 https://doi.org/10.1016/j.jallcom.2013.02.163

30. P.A. Shaikh, R.C. Kambale, A.V. Rao, Y.D. Kolekar, Effect of Ni doping on structural and magnetic properties of $Co_{1-x}Ni_xFe_{1.9}Mn_{0.1O4}$, J. Magn. Magn.Mater. 2010; 322: 718-726. https://doi.org/10.1016/j.jmmm.2009.10.048

31. Y. Huang, Y. Tang, J. Wang, Q. Chen, Mater. Chem. Phys. 2006; 97: 394. https://doi.org/10.1016/j.matchemphys.2005.08.035

32. M.E. Rabanal, A. Va´rez, B. Levenfeld, J.M. Torralba, J. Mater. Process. Technol. 143 (2003) 470. https://doi.org/10.1016/S0924-0136(03)00464-3

33. V.R.K. Murthy, B. Viswanathan, Ferrite Materials, Narosa Publishing House, 1990.

34. B. J. Madhu, E. Melagiriyappa, G. D. Prasanna, H. S. Jayanna and B.Nagappa " Dielectric studies on $Mg_xZn_{1-x}Fe_2O_4$ nanoparticles synthesized by combustion method" in, Synthesis and characterization of Nanostructured materials, Macmillan Advanced Research Series, Macmillan Publishers India Ltd., 2010, pp. 295-298. https://doi.org/10.4028/www.scientific.net/AMR.584.299

35. A. T. Raghavender and K. M. Jadhav, "Dielectric properties of Al-substituted Co ferrite nanoparticles", Bull. Mater. Sci., 2009; Vol. 32: pp. 575-578. https://doi.org/10.1007/s12034-

009-0087-8
36. K. Iwauchi, "Dielectric properties of fine particles of Fe_3O_4 and some ferries", Jap. J. Appli. Phys., 1971; Vol. 10: pp. 1520-1528

37. Koops CG. On the dispersion of resistivity and dielectric constant of some semiconductors at audio frequencies. Phys Rev. 1951; 83:121–124. https://doi.org/10.1103/PhysRev.83.121

38. Sivakumar P, Thyagarajan K, Gurusampath Kumar A, Obulapathi L, Effect of Mg doping on physical properties of Zn ferrite nanoparticles. J Aust Ceram Soci. 2018; 54: 467–473. https://doi.org/10.1007/s41779-018-0173-8

39. H. P. J. Wijin, and J. J. Went, The magnetization process in ferrites, Physica, 1951, Vol. 17 : pp. 976-99 https://doi.org/10.1016/0031-8914(51)90006-7

40. Murugesan, C., Perumal, M., Chandrasekaran, G.: Structural, dielectric and magnetic properties of cobalt ferrite prepared using auto combustion and ceramic route. Physica B, 2014; **448:** 53–56 https://doi.org/10.1016/j.physb.2014.04.055